Prospects for Measuring Neutral Gauge Boson Couplings in ZZ Production with the ATLAS Detector

S. Hassani

Laboratoire de l'Accélérateur Linéaire
IN2P3-CNRS et Université Paris-Sud, BP 34 , F91898 Orsay Cedex

Abstract

ZZ production at the LHC provides an opportunity to probe neutral gauge boson self-interaction in a direct way. The possibility to detect anomalous ZZZ and $ZZ\gamma$ couplings is investigated in the context of the ATLAS detector. The expected limits on these couplings will improve the limits currently obtained by the LEP experiments by 3 orders of magnitude.

ATL-PHYS-2003-022
16/07/2003

1 Introduction

The Standard Model (SM) of electroweak interactions makes precise predictions for the couplings between gauge bosons due to the non-abelian gauge symmetry of$SU(2)_L \otimes U(1)_Y$. These self-interactions are described by the triple gauge boson $WW\gamma$, WWZ, $Z\gamma\gamma$, $ZZ\gamma$ and ZZZ couplings and the quartic couplings. The study of vector pair production at the LHC provides sensitive ground for direct tests of the trilinear couplings. Deviations of the couplings from the SM values would indicate the presence of new physics beyond the SM [1]. The electroweak gauge boson couplings has been explored in great detail at LEP2 [2] and at the TeVatron [3]. No significant deviation from the SM prediction was seen for any of electroweak gauge boson coupling investigated.

While the charged boson couplings (TGC) already receive tree level SM contribution, the neutral trilinear gauge couplings (NTGC) do not; higher order corrections through virtual loops contribute at the level of 10^{-4}. New phenomena with characteristic mass scale above the present experimental threshold might lead to NTGCs in the effective Lagrangian [1, 5, 6] parameterizing the residual low energy effects from new physics. For example, as suggested in [5] virtual effects from new heavy fermions having non-standard coupling to gauge boson might generate sizeable anomalous couplings. One loop corrections in the SM and in supersymetric models [5], induce effective ZZV couplings which are of the $\mathcal{O}$ (10^{-4}).

Prospects for probing the charged sector have been studied in details at the LHC [4]. In this note a study of ZZ production at the LHC with the ATLAS detector is presented with the aim of searching for ZZZ and $ZZ\gamma$ anomalous couplings.
The note begins with a brief summary of the neutral trilinear couplings (NTGC) and their parametrization. A detailed analysis of the ZZ production and the signatures of the NTGCs at the LHC is then presented. Finally, a summary of the expected limits on anomalous couplings at the LHC with the ATLAS detector is given and compared with what will be obtained elsewhere.

2 Theoretical Framework

2.1 ZZZ and $ZZ\gamma$ Anomalous couplings

In the SM, at the parton level, the reaction $pp \to ZZ$ proceeds by the Feynman diagrams of figure 1 (t-channel graph exchange). The total SM ZZ production cross-section (with no cuts) is $\sim 12\,pb$. Anomalous couplings require the addition of the graphs shown in figure 2, which contribute to the ZZ production via a photon or Z in the s-channel.

In a model independent description there exist four couplings: two of them (f_4^Z, f_5^Z) describing the ZZZ vertex and two (f_4^γ, f_5^γ) parametrizing the $ZZ\gamma$ vertex. Assuming only Lorentz and $U(1)_{em}$ gauge invariance as well as Bose statistics, the most general

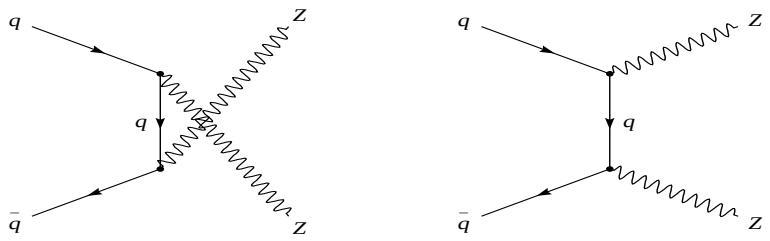

Figure 1: *The Feynman diagrams for the lowest order parton level contribution to the process* $pp \to ZZ$ *in the SM.*

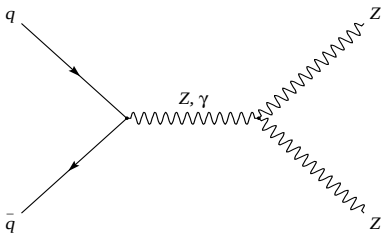

Figure 2: *Diagram for the anomalous process* $q\bar{q} \to ZZ$ *with* ZZZ *and* $ZZ\gamma$ *couplings*

ZZV vertex function [1, 5, 6] for on-shell Z's and off-shell $V(V = Z, \gamma)$ is given by:

$$, {}^{\alpha\beta\mu}_{ZZV} = \frac{\hat{s} - M_V^2}{M_Z^2}\Big[if_4^V(P^\alpha g^{\mu\beta} + P^\beta g^{\mu\alpha}) - if_5^V \epsilon^{\mu\alpha\beta\rho}(q_1 - q_2)_\rho\Big] \tag{1}$$

In the SM, at tree level, $f_4^V = f_5^V = 0$. The vertex functions vanish at $\hat{s} = M_V^2$ because of gauge invariance for $V = \gamma$, and Bose symmetry for $V = Z$. The couplings f_4^V is CP violating while f_5^V is CP conserving but violates parity.
Anomalous couplings contribute only to amplitudes with $(\lambda_1, \lambda_2) = (\pm, 0)$ where λ_1 and λ_2 are the helicities of the final Z's. The contribution of NTGCs to the amplitude is proportional to γ^3 (with $\gamma = \hat{s}/M_Z$), arising from the presence of dimension 6 operators (γ^2) and the necessity of one longitudinal final state boson ($\lambda = 0$) giving an additional factor γ [1]. One may remember [1] that in the charged TGC case, the TGC contribution to the amplitude is proportional to γ for $\Delta\kappa$ and γ^2 for λ and Δg_1.
The strong energy dependence via the γ^3 term provides a significant advantage at the LHC, where the high energy reach will enhance the sensitivity to non standard contributions.

2.2 Unitarity Limits and Form Factors

Neutral gauge couplings in ZZ production arise in the J=1 partial wave amplitude only (s-channel exchange of gauge-boson coupled to massless fermions). As seen above, the deviation from the SM prediction grows rapidly when $\hat{s}$ increases and may even reach an unreasonable (unitarity-violating) size. In order to cure this behavior, form factors decreasing with $\hat{s}$, relative to an arbitrary scale Λ_{FF}, are introduced. The form factor

typically used is [7]:

$$f_i^V(\hat{s}) = \frac{f_{i0}^V}{(1+\frac{\hat{s}}{\Lambda_{FF}^2})^n} \qquad (i=4,5), \tag{2}$$

where Λ_{FF} is related to the scale of the new physics producing the anomalous ZZV couplings. The exponent, n must be greater than 3/2 in order to ensure unitarity of the partial wave amplitudes [8, 9]. In the following, $n = 3$ will be assumed. Selecting an exponent sufficiently above the minimum value of 3/2 ensures that the ZZ differential cross section stays well below the unitarity limit at energies $\sqrt{\hat{s}} \gg \Lambda_{FF} \gg M_Z$, where novel phenomena such as resonance production are expected to dominate (and where this parameterization is clearly not correct). In the rest of the note, f_i^V denotes the bare coupling f_{i0}^V as defined in equation 2.

2.3 Event Generation

Next-to-leading order (NLO) calculations have shown [10] that the lowest order ($\mathcal{O}(\alpha_s)$) QCD corrections increase logarithmically with the center-of-mass energy. This is due to the opening of the $qg \to ZZq$ subprocess at $\mathcal{O}(\alpha_s)$ in conjunction with the increasing gluon density as function of the center-of-mass energy. This is similar to the enhancement of QCD corrections observed at large vector boson momenta in $W\gamma$, WZ and W^+W^- production. In $W\gamma$ and WZ production, the SM Born cross section is suppressed due to the appearancee of an exact or approximate radiation zero [16], while there is no radiation zero in the ZZ case.
Figure 3 shows the transverse momentum of the Z boson. NLO corrections are important at high $p_T(Z)$ and alter the shape of the distribution which tends to be enhanced at high $p_T(Z)$. Qualitatively, this is precisely what one expects from the non-standard $ZZ\gamma$ and ZZZ couplings and therefore the sensitivity to NTGCs will be decreased. Since the bulk of the large corrections at high $p_T(Z)$ come from events which contain a hard jet in the final state, a jet veto drastically reduces the size of the QCD corrections, and restores the sensitivity to the anomalous couplings [11].

The NLO generator by Dixon, Kunszt, and Signer [12] (DKS) for ZZ production includes contributions from the square of the Born graph, interferences between Born graphs and virtual one-loop diagrams, and the square of the real emissions graphs. The calculations take into account the full spin correlation in the vector boson production and decay (including the virtual one-loop graphs) in the narrow-width approximation. However, anomalous couplings are not taken into account. In the Monte Carlo program by Baur and Rainwater [9], the calculation is carried out at tree level including decay correlation and finite Z width effects but neglecting non-resonant Feynman diagrams. However, this generator includes the option of non-standard NTGC.
Neither generator takes into account the contribution from $gg \to ZZ$. The contribution from gluon fusion enhances the cross section by about 15% at the LHC [13], and is not taken into account in this note.
A comparison between the Baur/Rainwater and DKS leading order (LO)calculations was performed at particle level generators was performed using CTEQ4M (NLO) structure functions for the factorization scale $Q^2 = M_Z$. The chosen SM input parameters were:

$\sin^2\theta_W = 0.23$, $M_Z = 91.187\,GeV$, $\alpha_{EM}(M_Z) = 1/128$, the strong coupling constant $\alpha_S(M_Z) = 0.116$ and the leptonic branching ratio of the Z boson $BR(Z \to \ell^+\ell^-) = 3.36\%$. This comparison covers the channel $ZZ \to \ell_1^+\ell_1^-\ell_2^+\ell_2^-(\ell_{1,2} = e, \mu)$ with the following kinematic cuts: the transverse momentum of all the leptons must exceed $15\,GeV$, and the rapidity of all leptons must be less than 2.5. In the NLO case, a jet veto is applied: events where the transverse momentum of the additional parton exceeds $30\,GeV$ and the pseudo-rapidity of the parton satisfies $|\eta| < 3$ are rejected.
The transverse momentum distribution of the Z boson at LO (for the two generators), inclusive NLO and NLO with jet veto are shown in figure 3. The corresponding cross sections are shown in table 1.
At LO the two calculations are in excellent agreement for the total cross section and good agreement is seen for the shape of the distribution. The jet veto is effective in recovering the qualitative shape of the Born distribution.

The Baur/Rainwater LO events generator is interfaced to PYTHIA 6.1 [14] for the hadronization and the fragmentation of the partons and ATLFAST [16] for the fast detector simulation of the ATLAS experiment. Another comparison between the NLO result with a jet veto and the LO plus the parton shower result using the same jet veto is shown in figure 4. A reasonable agreement is found for the shape of the $p_T(Z)$ distribution.

Cross section	*Dixon/Kunszt/Signer*	*Baur/Rainwater*
σ_{Born}	22.1 fb	22.0 fb
$\sigma_{NLOinclusive}$	31.4 fb	-
$\sigma_{NLO0-jet}$	27.6 fb	-

Table 1: *Cross section prediction for* $ZZ \to \ell_1^+\ell_1^-\ell_2^+\ell_2^-(\ell_{1,2} = e, \mu)$ *from the two generators at LO, inclusive NLO and NLO with jet veto. A jet is defined for* $p_{\rm T}(jet) > 30\,GeV$, $|\eta(jet)| < 3$. *The statistical errors are 0.1 fb.*

3 Analysis

3.1 Event Selection

The event generation and simulation are based on the Baur/Rainwater LO Monte carlo interfaced to PYTHIA 6.1 and ATLFAST for the fast detector simulation of the ATLAS experiment. For all the numerical results, CTEQ4L parton distributions are employed, and the set of SM input parameters is chosen to be as in [9].

The $ZZ \to \ell^+\ell^-\ell'^+\ell'^-(\ell, \ell' = e, \mu)$ channel provides a clean signature. However, there are large reductible backgr ounds from the non-resonant $t\bar{t}$ and the $Zb\bar{b}$ events which contain a genuine Z in the final state. In addition, there is a background from ZZ production, where one of the Z decays into $\tau-$pair, with subsequent decays of the $\tau-$leptons, and the other Z decays into an electron or muon pair. The backgrounds events $Zb\bar{b}$ have

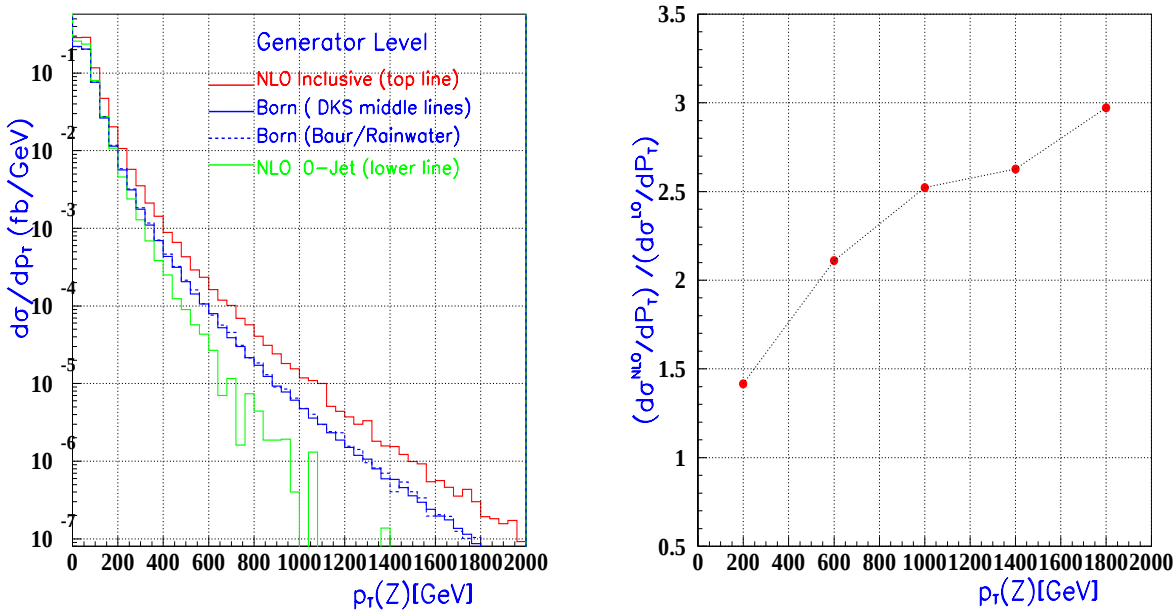

Figure 3: *Left: $p_T(Z)$ distribution (one entry per event) for $ZZ \to \ell_1^+\ell_1^-\ell_2^+\ell_2^-(\ell_{1,2} = e, \mu)$ production from Dixon/Kunszt/Signer and Baur/Rainwater superimposed at the Born level, inclusive NLO and NLO with a jet veto (defined as $P_T(jet) > 30\,GeV$, $|\eta(jet)| < 3$). Right: the ratio ofthe NLO differential cross section over the LO prediction.*

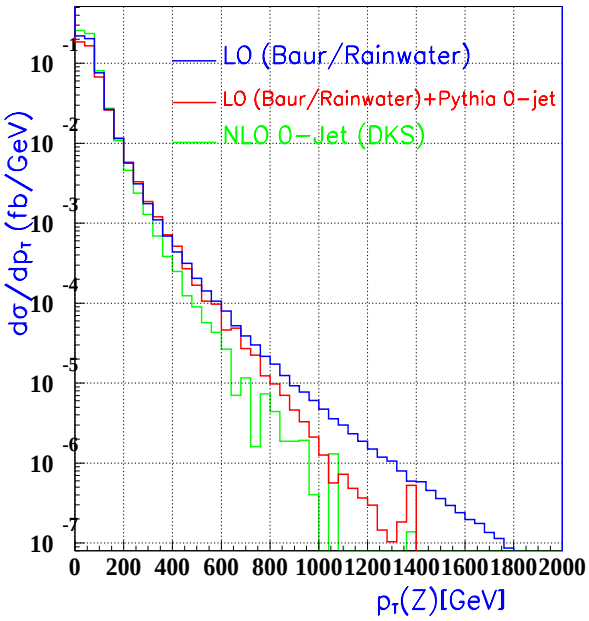

Figure 4: *$p_T(Z)$ distribution of $ZZ \to \ell_1^+\ell_1^-\ell_2^+\ell_2^-(\ell_{1,2} = e, \mu)$ for Baur/Rainwater LO with hadronization from PYTHIA with jet veto and NLO with the same jet veto.*

been generated using the AcerMC [17] (matrix element implementation of $gg \to Zb\bar{b}$ and $q\bar{q} \to Zb\bar{b}$ process to PYTHIA6.1).

The signal reconstruction proceeds by selecting four identified isolated leptons with $p_T >$ 20 GeV. This cuts rejects most of the $t\bar{t}$ background and $ZZ(\tau\tau)$ events. Both pair of leptons are required to have an invariant mass to be in the vicinity of the Z mass. This cut reduces the contributions from $t\bar{t}$ and $Zb\bar{b}$ cascade decays to 0.8 % of the signal. The $ZZ \to \ell^+\ell^-\ell'^+\ell'^-(\ell, \ell' = e, \mu)$ is essentially background free. The expected number of events after cuts (see table 2) for an integrated luminosity of 100 fb^{-1} is 780. The lepton efficiency was assumed to be 90% per lepton.

The advantage of the $ZZ \to \ell^+\ell^-\nu\bar{\nu}(\ell = e, \mu)$ channel is its larger branching ratio. The second Z boson gives a large missing energy to the event. The number of events after cuts expected for an integrated luminosity of 100 fb^{-1} is 5120, which is about a factor 6 larger than the number of charged lepton events. However, this channel suffers from large background coming mainly from $t\bar{t}$ and $Z + jets$ events.

Transverse Energy Lepton	$p_T^l > 20\,GeV$
Pseudo-rapidity Lepton	$\lvert\eta_l\rvert < 2.5$
Z mass constraint	$\lvert m_{l\bar{l}} - 91.2\rvert < 10\,GeV$
Missing Energy (for the $\ell\ell\nu\nu$ case only)	$p_T^{miss} > 50\,GeV$
Jet Veto	$p_T(jet) > 30\,GeV$ and $\lvert\eta(jet)\rvert < 3$

Table 2: *Summary of the selection requirements*

3.2 Background to $ZZ \to \ell^+\ell^-\nu\bar{\nu}$

The signal in this channel is characterized by two high p_T leptons from $Z \to \ell^+\ell^-$ decay and a large missing energy from $Z \to \nu\bar{\nu}$ decay. The production cross-section times branching ratio is $0.26\,pb$.
The largest background arises from reducible $Z + jets$ production, where large $\not{p}_T$ can be created by neutrinos or by badly reconstructed jets due to cracks, dead material and the limited calorimeter pseudo-rapidity coverage. In addition, the reducible backgrounds from $t\bar{t}$, Wt, $b\bar{b}$, W^+W^-/WZ and $Z \to \tau^+\tau^-$ have also to be considered.
The background events were generated using PYTHIA with the exception of single top production Wt, which was generated with ONETOP package [19].
Table 3 summarizes the relative importance of the various backgrounds using the ratio:

$$\frac{\sigma_B}{\sigma_S} = \frac{\sigma_{pp \to Process \to \ell^+\ell^- \not{p}_T}}{\sigma_{pp \to ZZ \to \ell^+\ell^- \not{p}_T}}$$

There will be a large rate of soft hadronic interactions (minimum-bias events) from the bulk of the proton-proton interactions. At high luminosity the pile-up of many soft interactions adds a non negligible level of noise on top of the interesting events. This can lead to fake jets and subsequent reduction of the signal due to the jet veto. However, it

Process	$t\bar{t}$	$b\bar{b}$	W^+W^-	WZ	Wt	$Z \to \tau^+\tau^-$	$Z + jets$
$\frac{\sigma_B}{\sigma_S}$	54	4×10^7	5.6	1.8	4.8	300	7000

Table 3: *Ratio of background to signal cross section before any cuts.*

has been shown in [23] that the effect of pile-up on jet veto when the threshold of the $p_T(jet) > 30\,GeV$ and $|\eta(jet)| < 3$ is smaller than 5%.

- $t\bar{t}$, $Wt(t \to bW)$: the subsequent decay of a top quark into a W boson and a b quark, followed by the W decay into $\ell\nu_\ell$ provide the same event signature as the $ZZ \to \ell^+\ell^-\ \not{p}_T$. Therefore, due to the very large top production cross section, these two processes represent a significant background. Since the top quark decays predominantly into the Wb final state, $t\bar{t}$ and Wt events are characterized by a large hadronic activity resulting in one or several high-p_T jets. This observation suggests that the $t\bar{t}$ and Wt backgrounds may be suppressed by vetoing the high-p_T jets. Such a "zero jet" requirement has been demonstrated to be very useful in reducing the size of the NLO QCD corrections in $pp \to ZZ + X$ production. The jet veto reduces also significantly the $t\bar{t}$ and Wt backgrounds as seen in table 4.

Process	ZZ	$Z + jets$	$t\bar{t}$	WZ	Wt	W^+W^-	$Z \to \tau^+\tau^-$
$p_T^l > 20\,GeV \quad \lvert\eta_l\rvert < 2.5$	11550	$366\ 10^5$	$5.466\ 10^5$	760	58180	55640	$1.9\ 10^5$
$\lvert m_{\ell\bar{\ell}} - 91.2\ GeV\rvert < 10\ GeV$	11210	$322.4\ 10^5$	75560	588	7580	7820	2810
$P_T^{miss} > 50\ GeV$	5530	$1.685\ 10^5$	51680	260	4490	2300	120
Jet Veto $(p_{jet}^T > 30\,GeV\ and \lvert\eta_{jet}\rvert < 3)$	5120	41640	2200	180	790	1560	60
$p_T(\ell^+\ell^-) > 150\,GeV$	580	12	10	10	3	0.5	0

Table 4: *Expected number of events for signal ($ZZ \to \ell^+\ell^-\nu\bar{\nu}$) and background after cuts for an integrated luminosity of* $100\ fb^{-1}$.

- $b\bar{b}$: The number of $b\bar{b}$ events is very large at the LHC, but the requirement of well isolated (from jets) leptons with high (greater than 20 GeV) transverse energy and large missing momentum suppresses this background.
- W^+W^-: The two W_s into leptons and neutrinos can have the same signature as the signal, however the Z mass constraint reduces this background.
- WZ: this background includes the case $W(\tau\nu_\tau)Z$ where the τ lepton decays into an electron or muon, and the case $W(e\nu)Z(ee)$, where the electron from the W decay is lost and gives rise to significant missing energy. This background is small.
- $Z(\tau^+\tau^-)$: this background arises from the cascade decay $Z \longrightarrow \tau^+\tau^- \longrightarrow \ell^+\ell^-\nu_l\bar{\nu}_l\nu_\tau\bar{\nu}_\tau$ in the WZ and $Z(\tau^+\tau^-)$ final state. This background is small because the decay of the τ lepton results in electrons or muons with significantly reduced p_T.
- $Z + jets$: this background is significant even when a jet veto is introduced and exceeds the signal for $p_T(\ell^+\ell^-) < 80\,GeV$ as shown in figure 7. However since the

$p_T(\ell^+\ell^-)$ distribution of the $Z + jets$, drops much faster than the distribution of the ZZ signal, a requirement of $p_T(Z) > 150\,GeV$ reduces this background to an acceptable level. This will not harm the sensitivity to anomalous coupling greatly as the anomalies only manifest themselves at high $p_T(Z)$.

Another source of background is the process $ZZ \longrightarrow \tau^+\tau^-\nu\bar{\nu} \longrightarrow \ell^+\ell^-\nu_l\bar{\nu}_l\nu_\tau\bar{\nu}_\tau\nu\bar{\nu}$. Although such cascade decay events are not really background events, they are not included in the Baur/Rainwater Monte carlo. It is expected to be further reduced by the p_T cuts on the final state leptons.
In table 4 the cuts applied to select $ZZ \to \ell^+\ell^-\nu\bar{\nu}$ are listed along with their effect on the signal and background. The rejection is enhanced by the jet veto. After all cuts about 580 events are expected for an integrated luminosity of $100\,fb^{-1}$, for $p_T(\ell^+\ell^-) > 150\,GeV$ (the region where the sensitivity to NTGCs is important) with 6% of background. The cuts lead to a tolerable background (figure 8) which is located away from the region of interest of the NTGCs searches. 2

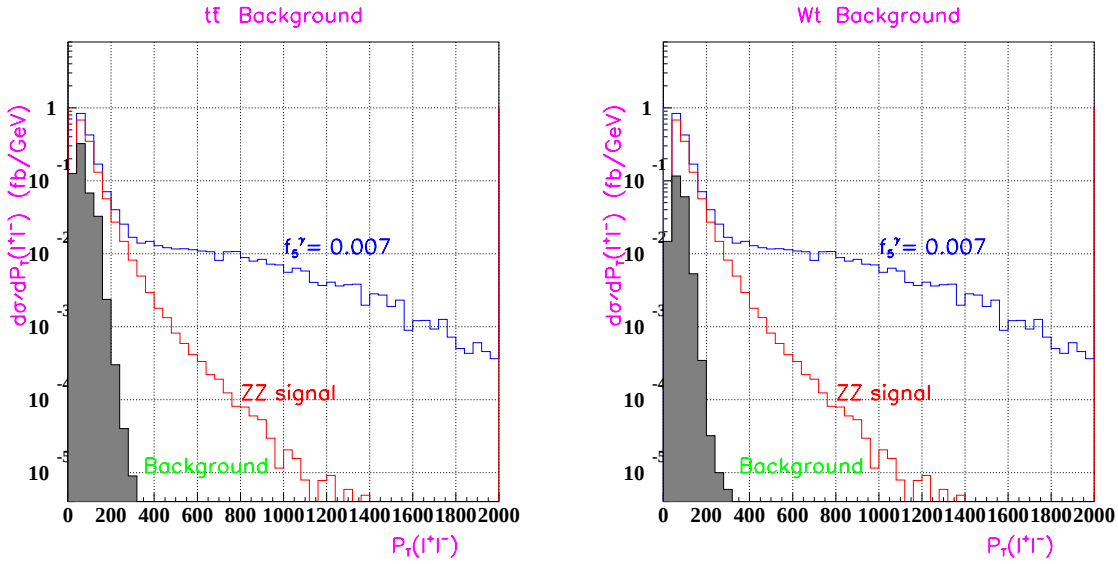

Figure 5: *Distribution of the transverse momentum of the lepton pair for the SM* $ZZ \to \ell^+\ell^-\nu\bar{\nu}(\ell = e, \mu)$ *signal, the backgrounds* $t\bar{t}$ *(left) and* Wt *(right) and the signal in presence of NTGC* $f_5^\gamma = 0.007$. *The cut on* $p_T(\ell^+\ell^-)$ *is not applied.*

3.3 Systematic uncertainties

The uncertainties on the predictions on event rates mainly come from the size of the generated samples, the parameterization of the cross section, the choice of the structure function the detector response and the luminosity. This will be describe below.
To determine the cross section dependency as a function of any pair of couplings, large samples of 500 000 events have been generated for different pairs of non zero NTGC values. The error on this parameterization was estimated by calculating the cross section for a

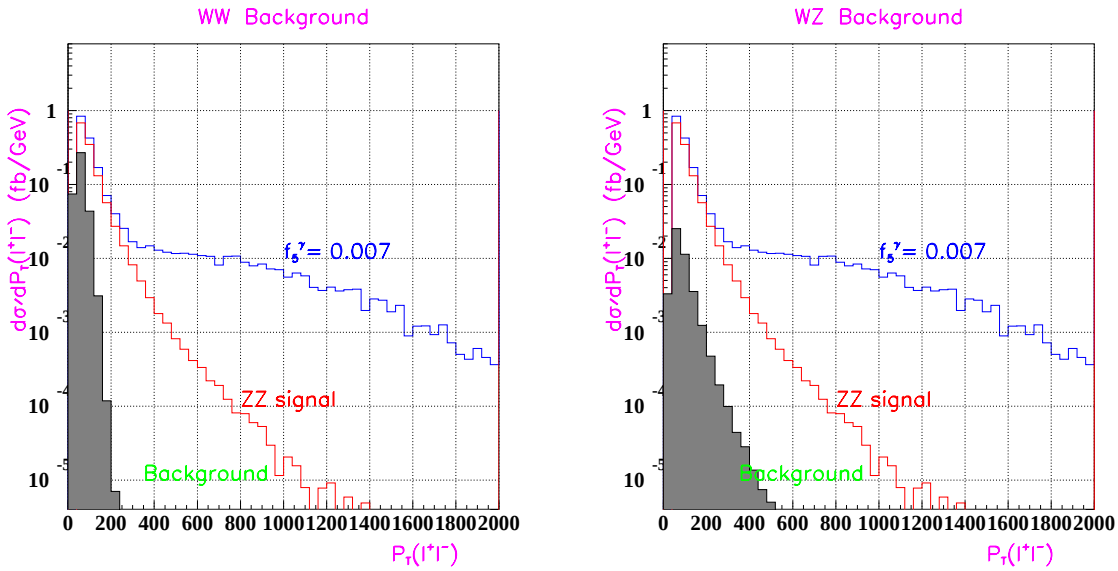

Figure 6: *Distribution of the transverse momentum of the lepton pair for the SM* $ZZ \to \ell^+\ell^-\nu\bar{\nu}(\ell = e, \mu)$ *signal, the backgrounds WW (left) and WZ (right) and the signal in presence of NTGC* $f_5^\gamma = 0.007$*. The cut on* $p_T(\ell^+\ell^-)$ *is not applied.*

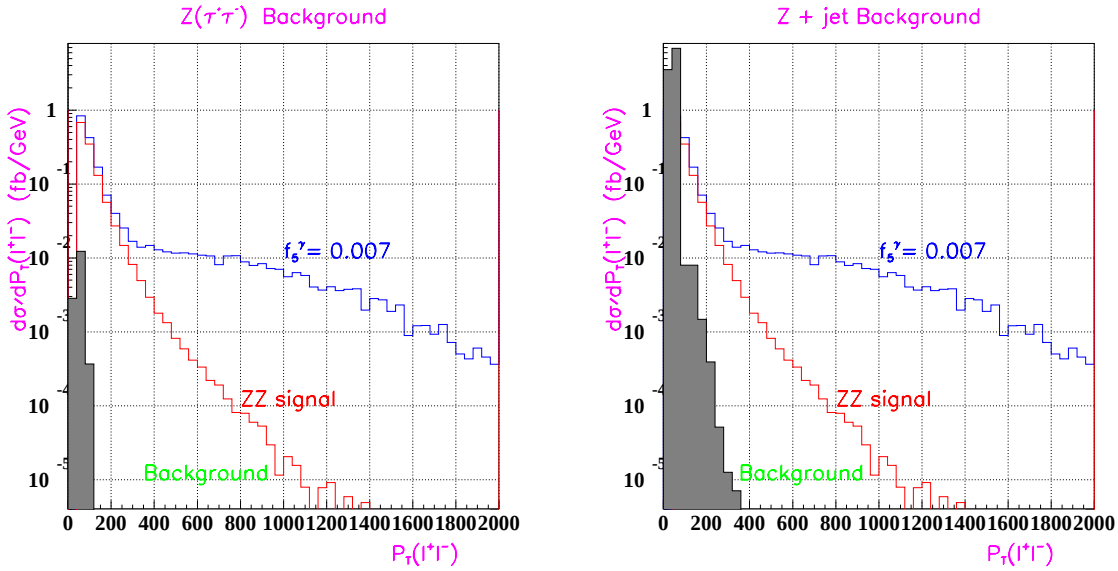

Figure 7: *Distribution of the transverse momentum of the lepton pair for the SM* $ZZ \to \ell^+\ell^-\nu\bar{\nu}(\ell = e, \mu)$ *signal, the backgrounds* $Z(\to \tau^+\tau^-)$ *(left) and* Z *+ jets (right) and the signal in presence of NTGC* $f_5^\gamma = 0.007$*.*

given pair of NTGCs and then comparing with the prediction from the parameterization. The error on this parameterization is 1%.
Two choices of the structure functions and of the scale can also affect the cross section and the $p_T(Z)$ distribution. The variation of the cross section for different structure functions is shown in figure 9. An error of 6% is used for the structure functions uncertainty. The uncertainty from the choice of scale is determined by varying the value of Q^2 (momentum

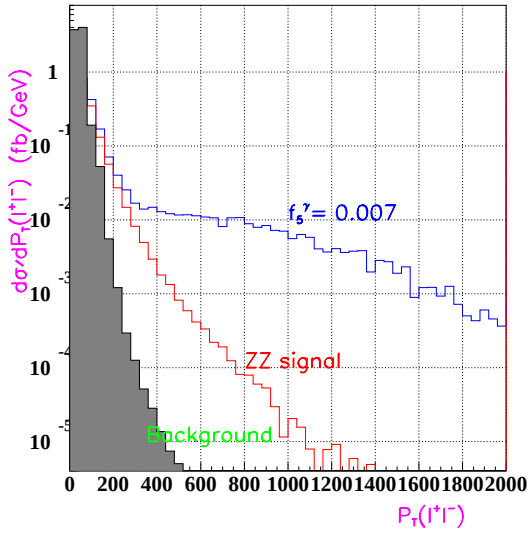

Figure 8: *Distribution of the transverse momentum of the lepton pair for the SM* $ZZ \to \ell^+\ell^-\nu\bar{\nu}(\ell = e, \mu)$ *signal, the sum of the backgrounds and for non standard value* $f_5^\gamma = 0.007$.

transfer) from $\hat{s}/2$ to $2\hat{s}$ the cross section was observed to change by 1%.
The electromagnetic energy scale for the detector and the energy resolution uncertainty and the resolution uncertainties are evaluated by changing the transverse momentum of the leptons by 5‰. A very small impact (less than 1%) on the sensitivity limit was found. The uncertainty on the luminosity was taken to be 5% [21]. The different sources of uncertainties are summarized in table 5. The uncertainty due to the errors on the background is negligible (see 4.3).

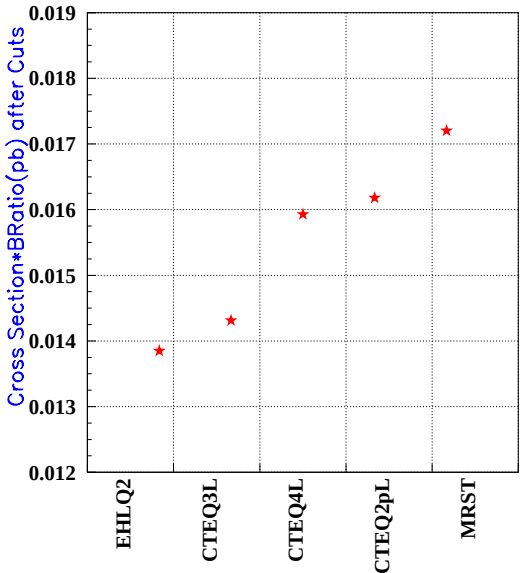

Figure 9: *Variation of the* ZZ *cross section production for different choices of parton density functions.*

Source of Error	Relative uncertainty
Luminosity	5%
Structure function choice	6%
Structure function scale	1%
Parameterization of the cross section and statistics of MC	1%
Total	8%

Table 5: *Summary of typical systematic uncertainties on the expected number of events*

3.4 Experimental Signatures of Anomalous ZZV couplings

Experimental sensitivity to NTGCs comes from three different types of information: the cross section, the energy dependence and the polarization.

3.4.1 Cross Section

It follows from the expression of the ZZV interaction vertex that the contributions from anomalous couplings to the cross sections are quadratic in f_i^V. The CP-conserving couplings always lead to real amplitudes interfering with the SM contribution. On the contrary, the CP-violating couplings always lead to purely imaginary amplitudes that do not interfere with the SM. Cross sections are therefore independent of the sign of f_V^4. Couplings with different CP-parity do not interfere with each other, so there are no cross-terms in the bilinear form which are proportional to the product of CP-conserving and CP-violating couplings. The total cross section as a function of two couplings can be expressed in the following bilinear form:

$$\sigma(f_i^V, f_j^{V'}) = \sigma_{SM} + a_0 f_i^V + a_1 (f_i^V)^2 + b_0 f_j^{V'} + b_1 (f_j^{V'})^2 + c f_i^V f_j^{V'} \qquad (3)$$

where σ_{SM} is the Standard Model cross section and a_i, b_i and c are some coefficients. Figure 10 shows the cross section of the process $ZZ \to e^+e^-\mu^+\mu^-$ as a function of the f_5^Z couplings. The counting measurement can be used to set limits on the anomalous couplings because of the pronounced rise of the total cross section for large non-zero couplings.

3.4.2 Energy Dependence

The effects of NTGCs are enhanced at large energies. This is a direct consequence of the high energy behavior of the NTGC contributions to the ZZ helicity amplitude which grows like $(\sqrt{\hat{s}}/M_Z)^3$. A typical signal of NTGCs will thus be a broad increase in the ZZ invariant mass distribution and the Z transverse momentum distribution. Figure 11 shows the enhancement of the ZZ production cross section for large values of the Z transverse momentum and the ZZ invariant mass in presence of NTGCs. Here and in all subsequent figures, only one NTGC is allowed to be non-zero at a time. CP-violating couplings and CP-conserving couplings have the same qualitative behavior at high transverse momenta

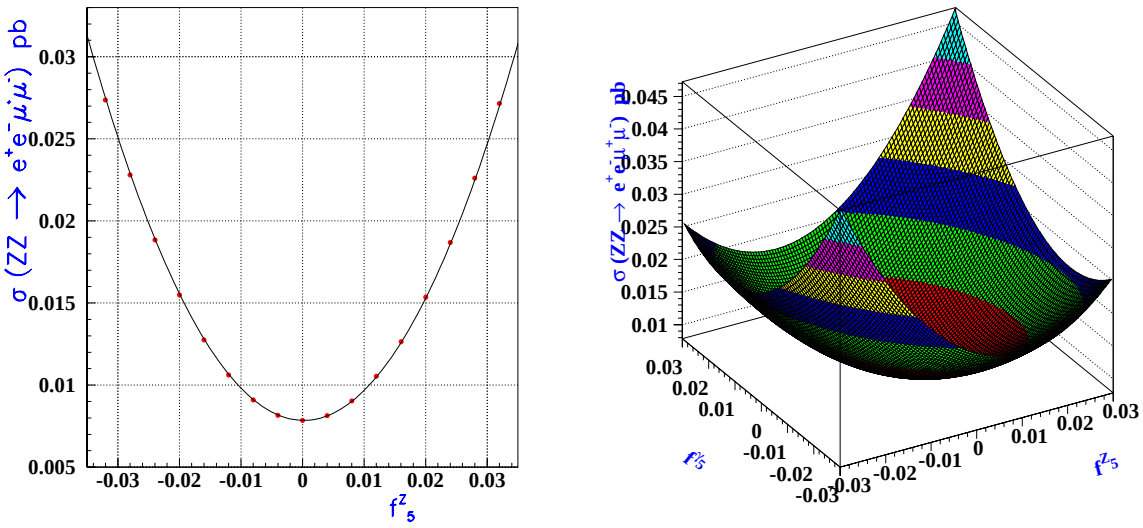

Figure 10: *The cross section for* $ZZ \to e^+e^-\mu^+\mu^-$ *as a function of* f_5^Z *couplings (left plot) and in the plane* (f_5^Z, f_5^γ) *(right plot). The solid line on the left plot is a fit with a simple bilinear function.*

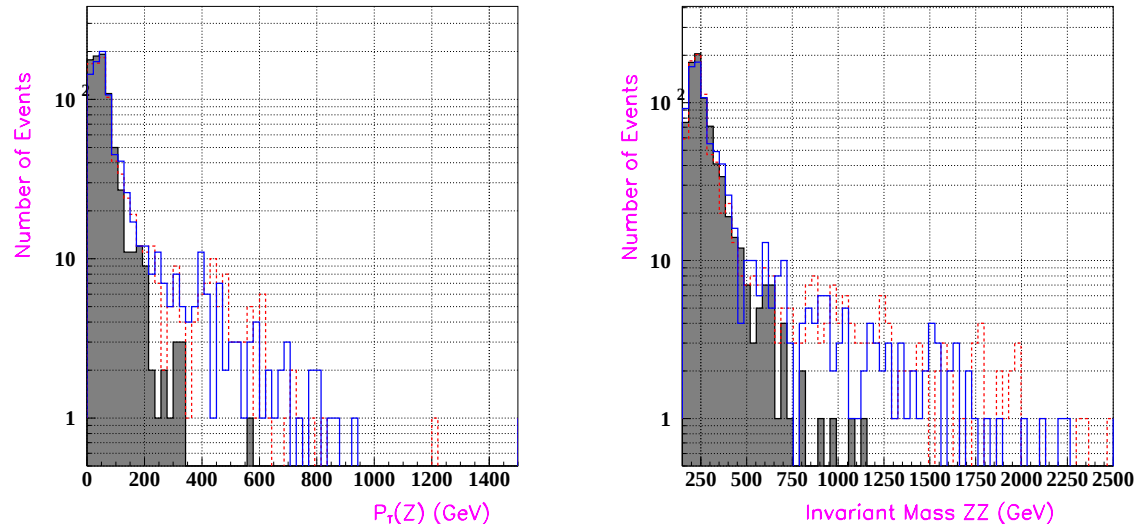

Figure 11: *Distribution of* $p_T(Z)$ *(left) and invariant mass of the two* Z_s *(right) for an integrated luminosity* $100\,fb^{-1}$*. The distributions are shown for the Standard Model (shaded histograms) and for* $f_5^Z = 0.02$ *(dashed histogram) and* $f_4^Z = 0.02$ *(solid histogram). A form factor of* $\Lambda_{FF} = 2\,TeV$ *was used.*

and high invariant masses. Thus it will be difficult to discriminate between the various NTGCs in these distributions because the magnitude of the interference effects is small.

3.4.3 Polarization

NTGCs lead to one transversely polarized and one longitudinally polarized Z boson. The polar angle θ^* of the leptonic decay products with respect to the Z direction contains information on the helicities of the vector bosons. Since the Z boson couplings to charged lepton is almost purely axial, transversely polarized Z bosons produce an $\sim (1+\cos^2\theta^*)$ distribution, while longitudinally polarized Z bosons yield a $\sin^2\theta^*$ distribution.
In the SM, the transverse polarization dominates the cross section as can be seen from the shape of the θ^* distribution shown in figure 12. This is to be expected since the $q\bar{q}$ annihilation process produces Z-boson pairs that are primarily transversally polarized [6], especially at large parton center-of-mass energy.
However, this effect is very small (see figure 13 for an integrated luminosity of 100 fb^{-1}) and the information from the energy dependence gives almost the full contribution on the limits.
Unlike the case of $W\gamma/WZ$, there is no radiation amplitude zero present in the ZZ production [11]. Therefore the boson production Θ has a smaller sensitivity to NTGCs than θ^* as seen in figure 12.

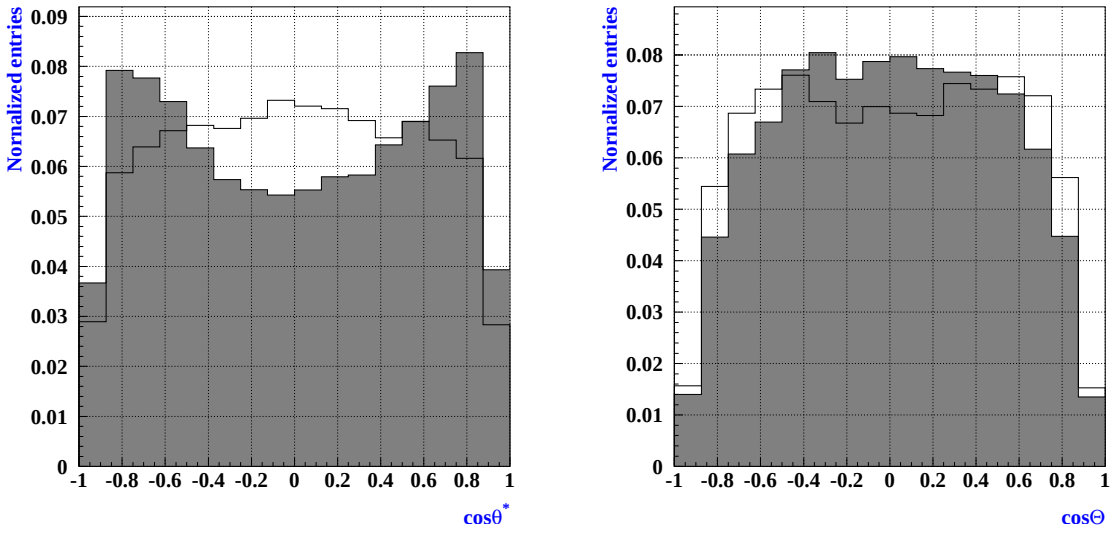

Figure 12: *Normalized distributions (with $p_T(Z) > 250\ GeV$, where the sensitivity to anomalous couplings is enhanced) for $ZZ \to \ell^+\ell^-\ell'^+\ell'^-(l,\ell' = e,\mu)$, of the decay angle θ^* (left) and of the production angle Θ (right). Distributions are shown for the Standard Model (shaded histograms) and for $f_5^Z = 0.02$ (white histograms). There are 2 entries per event*

The correlation between the maximum and minimum decay angles of the Z bosons is shown in figure 14 for the SM and in presence of NTGCs for $p_T(Z) > 250\ GeV$, where the sensitivity to NTGCs is important ($\theta_+ = Max(\theta_1^*,\theta_2^*)$ and $\theta_- = Min(\theta_1^*,\theta_2^*)$). In the presence of anomalous couplings the central region becomes populated because of the production of one longitudinally polarized Z and one transversely polarized Z. Although the expected number of events at the LHC will allow binning in two dimensions, a general multidimensional fit using all sensitive information will be difficult. For this reason, a

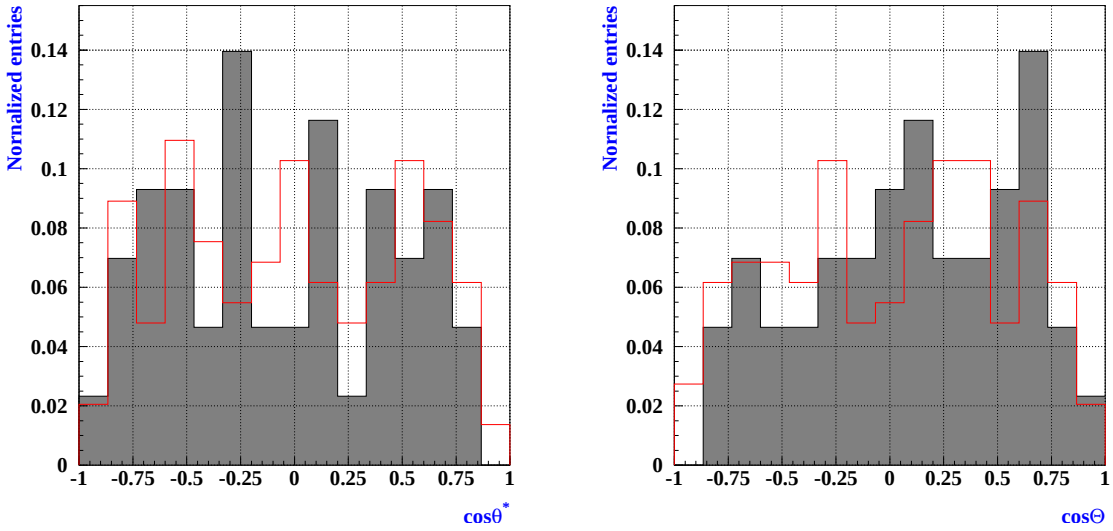

Figure 13: *Normalized distributions of the decay angle θ^* (left) and the production angle Θ (for $p_T(Z) > 250$) for an integrated luminosity 100 fb^{-1}. Distributions are shown for the Standard Model (shaded histograms) and for NTGC $f_Z^5 = 0.02$ (white histograms).*

variable R is constructed and defined as the ratio of the event probability in presence of NTGCs to that of the SM, as function θ_+ and θ_-.

$$R = \frac{P^{NTGC}(\theta_+, \theta_-)}{P^{SM}(\theta_+, \theta_-)}$$

R is constructed using Monte Carlo. According to the values of R, we define a variable $icat$ as:

$$icat = \begin{cases} 4 & \text{if } R > 1.2 \\ 3 & \text{if } 1.0 < R < 1.2 \\ 2 & \text{if } 0.8 < R < 1.0 \\ 1 & \text{if } R < 0.8 \end{cases}$$

The goal of this method is to project the information contained in the two dimensional distributions in a one dimensional variable, icat, plotted in figure 15 for the SM and in presence of NTGCs.
The angular correlation between the decay planes formed by the leptons defined by: $(\phi_1^* - \phi_2^*)$, where $\phi_{1,2}^*$ are the azimuthal angle decays in the rest-frame of the decaying bosons, is shown in figure 15. The sensitivity to NTGCs from the azimuthal decay angles is weak.

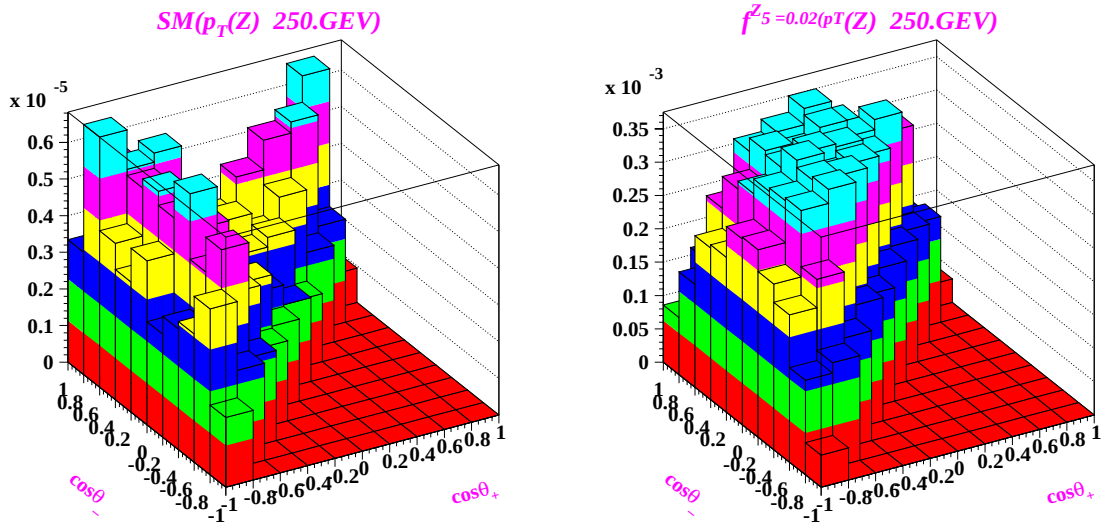

Figure 14: *Two-dimensional distribution of* $\cos\theta_+$ *as a function of* $\cos\theta_-$ *for* $P_T(Z) > 250$ *GeV in the SM (left plot) and in presence of NTGC* $f_5^Z = 0.02$

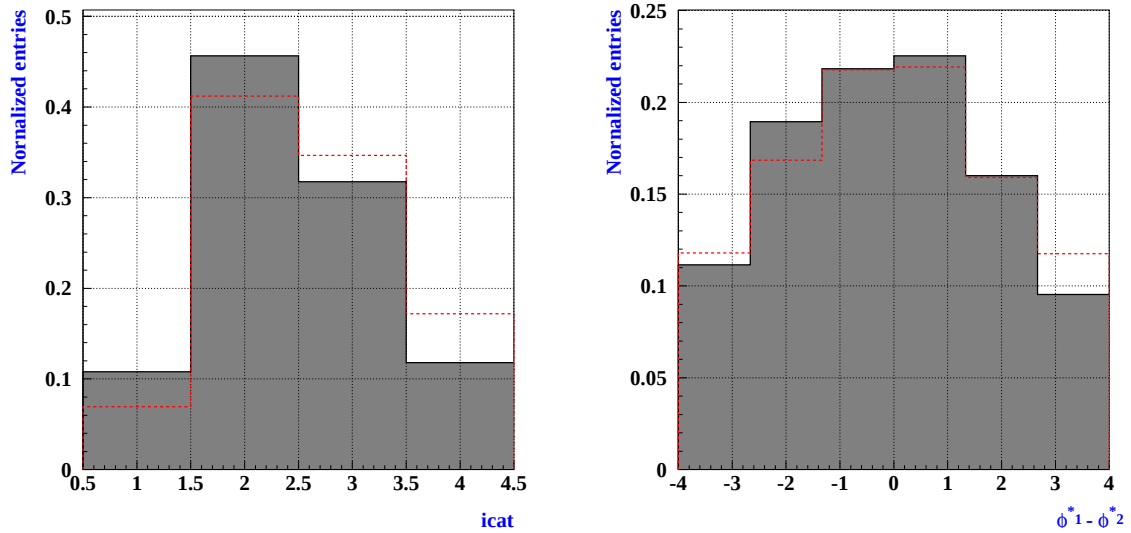

Figure 15: *Normalized distribution for icat (defined in the text) and* $\phi_1^* - \phi_2^*$. *Distributions are shown for the Standard Model (full histograms) and for NTGC* $f_5^Z = 0.02$ *(dashed histograms).*

4 Measurement of anomalous couplings

4.1 Impact of the Form Factor on the Sensitivity Limits

The magnitude of the effects of NTGCs depends on the scale and the power in the form factor as introduced in section 2.2. Since $f_{4,5}^V$ receive contributions only from operators

with dimension ≥ 6, the helicity amplitudes are proportional to $(\sqrt{\hat{s}}/M_Z)^3$. Deviations arising from non zero $f_{4,5}^Z$ are most visible at high invariant masses and therefore the effect of anomalous couplings is expected to grow with the form factor, Λ_{FF}. The higher the scale Λ_{FF} is, the more enhanced the cross section in presence of NTGCs will be. Similarly, a higher power than $n = 3\,(n = 4)$ leads to less additional events at invariant masses above Λ_{FF} as shown in figure 16.

The derived limits on anomalous couplings depends on the form factor Λ_{FF}, as illustrated

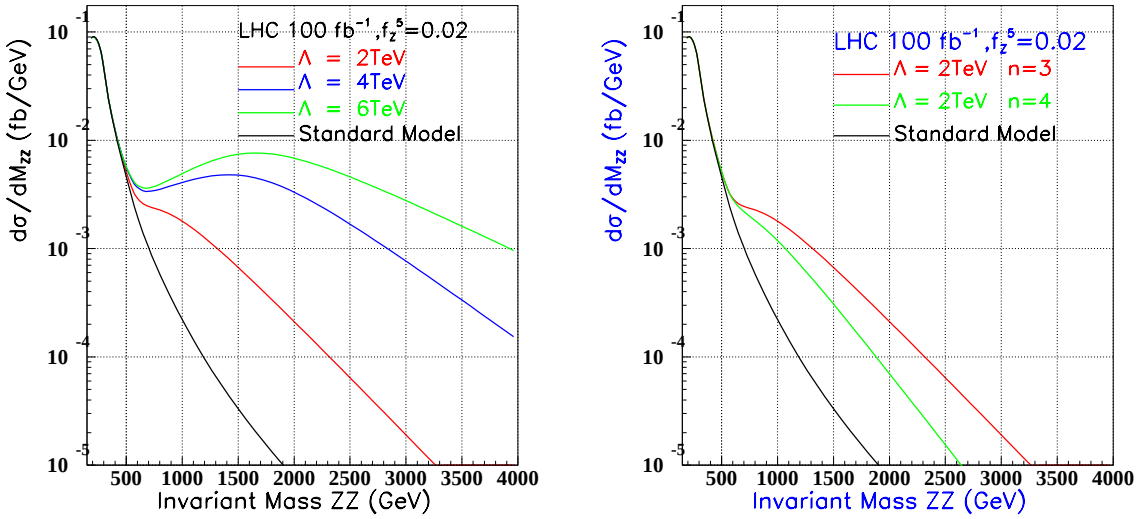

Figure 16: *Reconstructed invariant mass for* $ZZ \to \ell^+\ell^-\ell'^+\ell'^-(\ell,\ell' = e,\mu)$ *is plotted for the Standard Model and various choices of the generalized dipole form factor parameterization* Λ_{FF} *(left) and the power* n *(right) with the coupling* $f_5^Z = 0.02$

.

in figure 17, where the confidence limits for f_5^Z couplings are presented as a function of Λ_{FF}, for a dipole form factor with $n = 3$. The limits are obtained using a maximum likelihood fit to the $p_T(Z)$ distribution (see section 4.2.2). The unitarity limit given by [9]:

$$|f_{4,5}^Z| < \frac{0.089TeV^3}{\Lambda_{FF}^3} \frac{(\frac{2}{3}n)^n}{(\frac{2}{3}n-1)^{(n-\frac{3}{2})}} \tag{4}$$

$$|f_{4,5}^\gamma| < \frac{0.11TeV^3}{\Lambda_{FF}^3} \frac{(\frac{2}{3}n)^n}{(\frac{2}{3}n-1)^{(n-\frac{3}{2})}} \tag{5}$$

is also shown in figure 17. Anomalous couplings larger than these limits violates unitary. An example of the limits obtainable from a simultaneous determination of a pair of NTGCs (f_5^Z, f_4^Z) from a fit to the $P_T(Z)$ distribution, is shown in figure 17. In this case the unitary limit is presented by a circle. As shown in figure 17, limits depend strongly on the form factor scale.

If no deviations from the Standard Model are seen, and in the absence of any direct observation of new physics limits have to be set on the NTGCs. The question is then: since the form factor is unknown, what is the appropriate choice of scale ?[22].

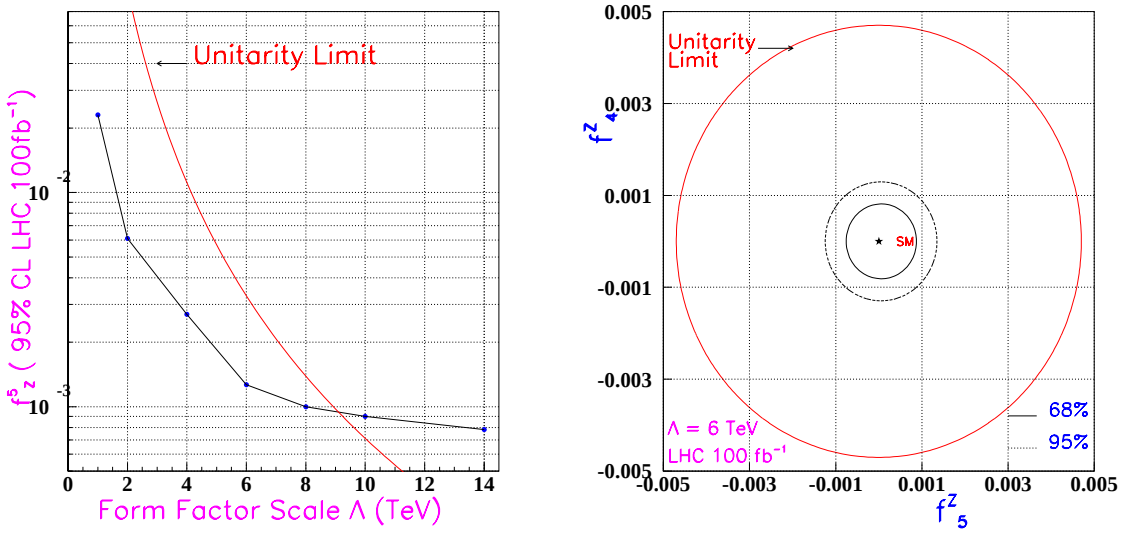

Figure 17: *Limits on f_5^Z couplings at the 95% confidence level as a function of Λ_{FF} for $n = 3$ (left). The plot to the right shows 68% and 95% contour limits in the plane of (f_5^Z, f_4^Z) for $\Lambda_{FF} = 6\,TeV$. The plots have been made from a binned maximum likelihood fit to the $p_T(Z)$ distribution of $ZZ \to \ell^+\ell^-\ell'^+\ell'^-(\ell, \ell' = e, \mu)$ at an integrated luminosity of 100 fb^{-1}*

.

Ideally, the limits should be given as a function of the scale Λ_{FF}. If the choice of Λ_{FF} is below the "INTRINSIC" scale of the data, the sensitivity relies on a too small assumption and the effects of NTGCs at a high scale will be undererestimated. Moreover, the analysis will depend on the choice of the scale since the sensitivity then lies in different regions of phase-space. The choice of scale should reflect the potential of the machine, the detector and the analysis.
At high Λ_{FF}, there is asymptotic limit because of machine, energy and luminosity limitations convoluted with analysis sensitivity. For the LHC, this occurs at about $\Lambda_{FF} = 6\,TeV$ with some variation for the type of coupling.

4.2 Limits on the anomalous couplings

In this section two methods to set limits on anomalous couplings will be presented :a counting method and a likelihood fit to NTGC sensitive kinematical variables. In deriving the sensitivity limits, only channels with electrons and muons in the final state are considered.

4.2.1 Limits from the total cross section measurement

As previously pointed out, the number of events (cross section) increases for couplings different from the SM values, especially at high $p_T(Z)$ as shown in figure 11. Therefore, the analysis can be more sensitive to NTGCs if an appropriate threshold on $p_T(Z)$ is set in order to strongly suppress SM and background events. The merit of such a cut is to enhance a region of phase-space with high sensitivity to NTGCs.
Limits on the anomalous couplings f_i^V from event counting above a certain $p_T(Z)$ threshold can be derived by solving the equation:

$$N_{predicted}(f_i^V, f_j^{V'}) = N(\alpha) \tag{6}$$

defining an ellipse in the $(f_i^V, f_j^{V'})$ plane, with N(α) the upper limit at a given confidence level α on the number of observed events derived from Poisson probability.

$$P = \frac{e^{-\mu}\mu^N}{N!}$$

where μ is the expected number of SM events given by the following relation:

$$\mu = b + \varepsilon\sigma(f_i^V, f_j^V)\mathcal{L} \tag{7}$$

where b is the expected background, $\mathcal{L}$ is the total integrated luminosity, ϵ is the efficiency deduced from Monte Carlo, and σ is the cross section.
The systematic uncertainties due to background, efficiency and luminosity are taken into account by convoluting the Poisson probability of events observed with Gaussian distributions for luminosity, efficiencies and background. The rms of these Gaussian probabilities is taken from table 5.
The 95% confidence limits are summarized in table 6 for $ZZ \to \ell^+\ell^-\ell'^+\ell'^-(\ell, \ell' = e, \mu)$ for six different $p_T(Z)$ thresholds. In setting the confidence limits, the negative log likelihood is used (ln L = - log P). The 95% confidence limit is taken as $\Delta\ell nL = 1.92$.
The limits from cross section measurement method are relatively easy to obtain. The extra kinematical information from, for instance, the $p_T(Z)$ spectrum is ignored.

4.2.2 Limits from kinematical information

A more sophisticated method is to fit the shape of kinematical distributions which are sensitive to NTGCs. This method usually provides tighter limits since it uses additional information contained in these distributions, and is less sensitive to the overall normalization factor.
The expected data set was simulated by Poisson-fluctuating the predicted number of events in each bin of the Standard Model of the Z boson distribution after the fast detector simulation, in order to account for statistical fluctuations . The reference distributions are obtained for different values of the couplings using that the cross section is a quadratic function of the anomalous couplings (see equation 3). One may write the cross section $\sigma(f_i^Z, f_i^\gamma)$ as a function of the cross section calculated for six distinct combinations of f_i^Z

$P_T(Z)$ *cut*	*Expected SM events*	f_5^γ	f_4^γ	f_5^Z	f_4^Z
100	*160*	*[-0.0043, 0.0045]*	*[-0.0030, 0.0030]*	*[-0.0033, 0.0036]*	*[-0.0026, 0.0026]*
200	*27*	*[-0.0028, 0.0025]*	*[-0.0024, 0.0024]*	*[-0.0022, 0.0024]*	*[-0.0019, 0.0019]*
300	*7*	*[-0.0025, 0.0022]*	*[-0.0021, 0.0021]*	*[-0.0021, 0.0021]*	*[-0.0017, 0.0017]*
400	*3*	*[-0.0021, 0.0019]*	*[-0.0018, 0.0018]*	*[-0.0019, 0.0018]*	*[-0.0016, 0.0016]*
500	*1*	*[-0.0018, 0.0019]*	*[-0.0017, 0.0017]*	*[-0.0018, 0.0016]*	*[-0.0015, 0.0015]*
600	*0*	*[-0.0017, 0.0019]*	*[-0.0016, 0.0016]*	*[-0.0017, 0.0016]*	*[-0.0014, 0.0014]*

Table 6: *Limits on NTGCs at 95% confidence level as a function of $P_T(Z)$ cut using the counting method.*

and f_i^γ value as follows:

$$\begin{aligned}\sigma(f_i^Z, f_i^\gamma) = {} & (1 - (\frac{f_i^Z}{f_{i1}^Z})^2 - (\frac{f_i^\gamma}{f_{i1}^\gamma})^2 + \frac{f_i^Z f_i^\gamma}{f_{i1}^Z f_{i1}^\gamma})\sigma(0,0) - (\frac{f_i^\gamma}{2f_{i1}^\gamma} - \frac{1}{2}(\frac{f_i^\gamma}{f_{i1}^\gamma})^2)\sigma(-f_{i1}^\gamma, 0) \\ & + (\frac{f_i^\gamma}{2f_{i1}^\gamma} + \frac{1}{2}(\frac{f_i^\gamma}{f_{i1}^\gamma})^2 - \frac{f_i^Z f_i^\gamma}{f_{i1}^Z f_{i1}^\gamma})\sigma(f_{i1}^\gamma, 0) - (\frac{f_i^Z}{2f_{i1}^Z} - \frac{1}{2}(\frac{f_i^Z}{f_{i1}^Z})^2)\sigma(0, -f_{i1}^Z) \\ & + (\frac{f_i^Z}{2f_{i1}^Z} + \frac{1}{2}(\frac{f_i^Z}{f_{i1}^Z})^2 - \frac{f_i^Z f_i^\gamma}{f_{i1}^Z f_{i1}^\gamma})\sigma(0, f_{i1}^Z) + \frac{f_i^Z f_i^\gamma}{f_{i1}^Z f_{i1}^\gamma}\sigma(f_{i1}^\gamma, f_{i1}^Z)\end{aligned} \tag{8}$$

In the program $f_{i1}^Z = 3.$ and $f_{i1}^\gamma = 3$ were set.
The likelihood function is calculated as in the case of the counting method. For each p_T bin a Poisson likelihood is given as:

$$P_i = \frac{e^{-(b_i + \varepsilon\sigma_i\mathcal{L})}(b_i + L\varepsilon\sigma_i)^{n_i}}{n_i!}, \tag{9}$$

where n_i is the number of observed events in the i^{th} bin and σ_i is given by the equation 8. Therefore, the probability of observing the given distribution assuming uncorrelated bins is given by the following relation:

$$P = \prod_{i=1}^{N_b} P_i,$$

where N_b is the number of bins in the histogram. The negative log likelihood is given by:

$$L = -\ln P = -\sum_{i=1}^{N_b}(n_i \ln(b_i + \varepsilon\sigma_i\mathcal{L}) - (b_i + \varepsilon\sigma_i\mathcal{L})) \tag{10}$$

where coupling independent terms have been omitted.

In order to determine the sensitivity to NTGCs, the $p_T(Z)$ spectrum is used for the $ZZ \to \ell^+\ell^-\nu\bar{\nu}$ channel. For the $ZZ \to \ell^+\ell^-\ell'^+\ell'^-$ channel, the $p_T(Z)$ distribution, and three other sets of variables, (M^{inv}_{ZZ}, Θ), $(p_T(Z), \theta^*)$ and $(p_T(Z), icat)$, where Θ is the production angle, θ^* is the decay angle and $icat$ is an integer variable describing polarization, are used. These sets of observables consist of one variable sensitive to the energy behavior and one sensitive to angular information.

4.3 Results

The expected limits at 95% confidence level on the NTGCs obtained from fits to binned distributions of various observables are listed in table 7 and 8, for an integrated luminosity of 100 fb^{-1} and with the form factor, $\Lambda_{FF} = 6\,TeV$. Only one NTGC is allowed to vary each time while the other couplings are set to their standard model values. The limits are obtained averaging over a large number ($\sim$ 10000) of LHC "experiments" (simulated data samples). Figure 18 shows an example for one LHC "experiment".

couplings	$p_T(Z)$	(M^{inv}_{ZZ}, Θ)	$(p_T(Z), \theta^*)$	$(p_T(Z), icat)$
f_5^Z	*[-0.0014, 0.0012]*	*[-0.0010, 0.0015]*	*[-0.0011, 0.0015]*	*[-0.0012, 0.0013]*
f_4^Z	*[-0.0012, 0.0012]*	*[-0.0011, 0.0012]*	*[-0.0011, 0.0012]*	*[-0.0012, 0.0011]*
f_5^γ	*[-0.0016, 0.0014]*	*[-0.0014, 0.0015]*	*[-0.0013, 0.0015]*	*[-0.0012, 0.0017]*
f_4^γ	*[-0.0014, 0.0014]*	*[-0.0012, 0.0016]*	*[-0.0015, 0.0013]*	*[-0.0013, 0.0014]*

Table 7: *95% confidence level intevals* ($\Delta(\ln\mathcal{L}) = 1.92$) *in the* $ZZ \to \ell'^+\ell'^-\ell^+\ell^-$ ($\ell, \ell' = e, \mu$) *case from one dimensional fits (one coupling varied) assuming an integrated luminosity of* 100 fb^{-1} *and averaging over 10000 LHC experiments.*

couplings	$\mathcal{L} = 10\,fb^{-1}$	$\mathcal{L} = 100\,fb^{-1}$
f_5^Z	*[-0.0013, 0.0012]*	*[-0.00066, 0.00063]*
f_4^Z	*[-0.0014, 0.0014]*	*[-0.00064, 0.00064]*
f_5^γ	*[-0.0015, 0.0017]*	*[-0.00075, 0.00077]*
f_4^γ	*[-0.0015, 0.0015]*	*[-0.00075, 0.00075]*

Table 8: *95% confidence level intervals* ($\Delta(\ln\mathcal{L}) = 1.92$) *in the* $ZZ \to \ell^+\ell^-\nu\bar{\nu}$ ($\ell = e, \mu$) *case, from one dimensional fits (one couplings varied) to the* $p_T(Z)$ *spectrum, assuming an integrated luminosity of* 10 fb^{-1} *and* 100 fb^{-1} *and averaging over 10000 LHC experiments.*

The most stringent bounds are obtained from the $ZZ \to \ell^+\ell^-\nu\bar{\nu}(l = e, \mu)$ channel, where the statistical sensitivity is of the order $\mathcal{O}$ (0.0007) for $f^V_{5,4}(V = Z, \gamma)$. The $ZZ \to \ell^+\ell^-\ell^+\ell^-(l = e, \mu)$ channel yields a sensitivity which is a factor 2 weaker. For comparison the sensitivities achievable for the $ZZ \to \ell\ell\nu\nu(\ell = e, \mu)$ channel for an integrated luminosity of 10 fb^{-1}, corresponding to 1 year at low luminosity are listed in table 8 and are of the order $\mathcal{O}$ (0.001).

Combining the limits from the two different channels will result in a small improvement of the bounds as listed in table 9.
The sensitivity to NTGCs lies mainly in high-end energy spectrum with a very small contribution from the angular information.
The difference in sensitivity between $f_{5,4}^{Z}$ and $f_{5,4}^{\gamma}$ couplings is due to differences in the differential cross section at high energies between ZZZ and $ZZ\gamma$ contributions which depend on the$Zf\bar{f}$ and $\gamma f\bar{f}$ couplings and the parton distribution functions.
Multi-parameter fits show a large correlation (50%) between f_5^Z and f_5^γ and between f_4^Z and f_4^γ. The f_5^V and f_4^V couplings do not interfere, as expected from the CP-odd nature of f_4^V and CP-even nature of f_5^V. This is illustrated in figure 19 which shows a 68% ($\Delta(\ln\mathcal{L}) = 1.15$) and 95% ($\Delta(\ln\mathcal{L}) = 3.0$) confidence level regions (using a fit of the $p_T(Z)$ spectrum) for the $ZZ \to \ell'^+\ell'^-\ell^+\ell^-(\ell,\ell' = e,\mu)$ channel for an integrated luminosity of $100\,fb^{-1}$.

couplings	$p_T(Z)$ $\mathcal{L} = 100\,fb^{-1}$
f_5^Z	*[-0.00063, 0.00062]*
f_4^Z	*[-0.00062, 0.000062]*
f_5^γ	*[-0.00073, 0.00074]*
f_4^γ	*[-0.00073, 0.00073]*

Table 9: *95% confidence level limits* ($\Delta(\ln\mathcal{L}) = 1.92$) *combined intervals from the two channels* $ZZ \to \ell^+\ell^-\nu\bar{\nu}$ $(\ell = e,\mu)$ *and* $ZZ \to \ell'^+\ell'^-\ell^+\ell^-$ $(\ell,\ell' = e,\mu)$, *assuming an integrated luminosity of* $100\,fb^{-1}$ *and averaging over 10000 LHC experiments.*

The systematics uncertainties are evaluated by changing the model assumption in the "simulated data sample" while leaving the reference (Monte Carlo model used in the fit) unchanged. The shifts in the central NTGC value determined in 10000 LHC experiments is taken as the systematic error in each case and the effect on the limit is obtainaed by convoluting the Poisson probabilities used in the likelihood with Gaussian with a rms obtained by this shift. The effect is negligible. However, one can note that the net effect of this change (without convolution) is typically 10%.
For the $ZZ \to \ell\ell\nu\nu$ channel the background for $p_T(Z) > 150\,GeV$ is less than 10% of the signal with an error of about 30% giving a small (less than 3%) uncertainty, with a negligible effect on the limits.

In summary, the best limits on the NTGCs are obtained when kinematical information, such as the $p_T(Z)$ distribution, is included. Adding angular information gives only a marginal improvement as the dominant sensitivity arises from the energy dependence. In addition, limits from the counting method depends on the optimization of the selected phase-space regions, as illustrated for $p_T(Z)$ in figures 16, 20 and 21, where most of the sensitivity to the anomalous couplings is contained in a few high $p_T(Z)$ events.

4.4 Measuring Form Factors

In the event that significant non-zero NTGCs are observed, the structure and the scale of the form factor must be determined in order to have meaningful results. In reference [5], it was pointed out that one can in principle determine the form factor by measuring the $\sqrt{\hat{s}}$ distribution of the NTGC measured. A detailed study of the method was performed for $W(\rightarrow e\nu, \mu\nu)\gamma$ study at the LHC in [4].
It is indeed possible to measure the energy dependence of anomalous couplings by grouping the data into bins of invariant mass and extracting constant anomalous couplings in each bin. Subsequent the form factor parametrization can be determined from a fit to the NTGC dependency with energy. The method is illustrated in figure 22 for the case of the $ZZ \rightarrow 4leptons$, after detector simulation and applying selection cuts.

For the example shown in figure 22, the dataset was produced with an anomalous couplings $f_5^Z = 0.06$ described by an $n = 3$ dipole form factor and $\Lambda_{FF} = 2\,TeV$. A sample of events, corresponding to three years of high luminosity ($300\,fb^{-1}$) is binned according to the reconstructed invariant mass. A measurement of NTGCs is performed within each domain using a binned maximum likelihood fit to the $p_T(Z)$ distribution. The results of the likelihood fits are plotted as a function of the invariant mass and a fit using the form factor of equation (2) is performed. The bare coupling and the form factor scale are reconstructed to be $f_{50}^Z = 0.061 \pm 0.003$ and $\Lambda = 2.07 \pm 0.05$, i.e. they can be measured with a relative precision of about a percent. The central values of the reconstructed parameters are compatible with the input parameters.
As the $ZZ \rightarrow \ell\ell\ell\ell$ can be fully reconstructed, the possible precision in the form factor determination is expected to be better than that from $ZZ \rightarrow \ell\ell\nu\nu$,$WZ$ and $W\gamma$ final states, which relies on a precise p_T(miss) determination.
If non-zero anomalous couplings are observed, the method provides indirect information about the dynamics of the underlying new physics.

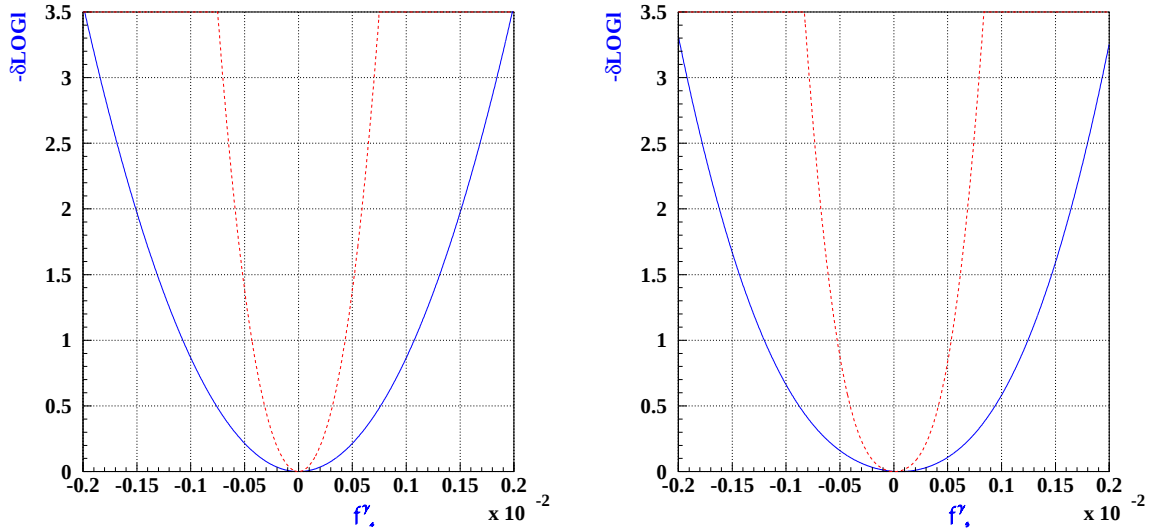

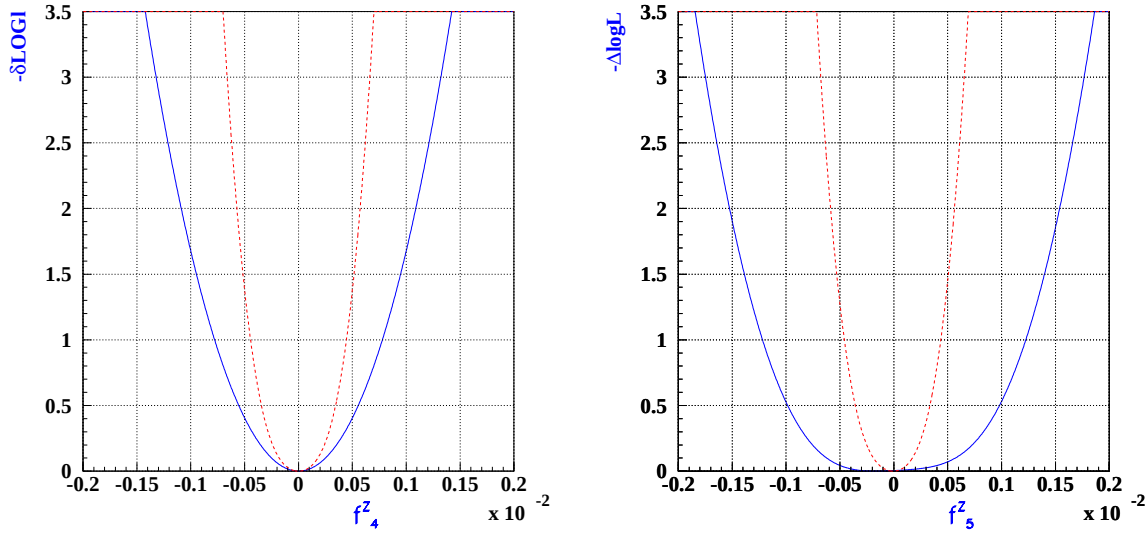

Figure 18: *An example of log-likelihood curves for "one typical LHC experiment" for an integrated luminosity of* 100 fb^{-1} *in the* $ZZ \to \ell^+\ell^-\ell^+\ell^-(l = e, \mu)$ *channel (solid curve) and in the* $ZZ \to \ell^+\ell^-\nu\bar{\nu}(\ell = e, \mu)$ *(dashed curve) .*

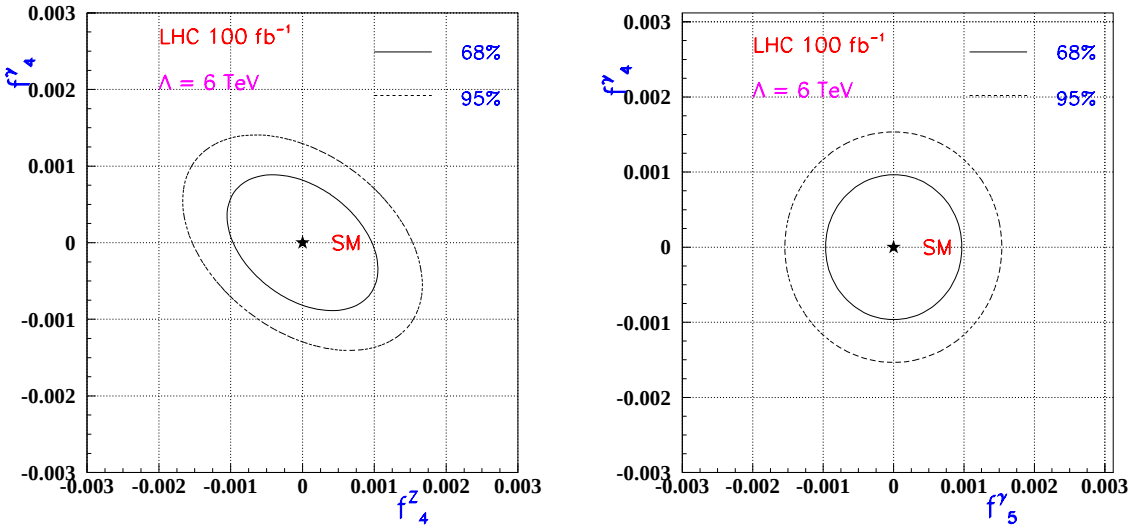

5 Conclusion

For an integrated luminosity of 100 fb^{-1}, neutral triple gauge boson bare couplings can be measured at the LHC with an accuracy of down to 7.10^{-4} assuming a form factor scale of $\Lambda_{FF} = 6\,TeV$. This sensitivity limit can be compared with the bounds from recent measurements at LEP2 [2]:

$$-0.31 < f_4^Z < 0.29 \qquad -0.17 < f_4^\gamma < 0.19$$

$$-0.19 < f_5^Z < 0.20 \qquad -0.36 < f_5^\gamma < 0.40$$

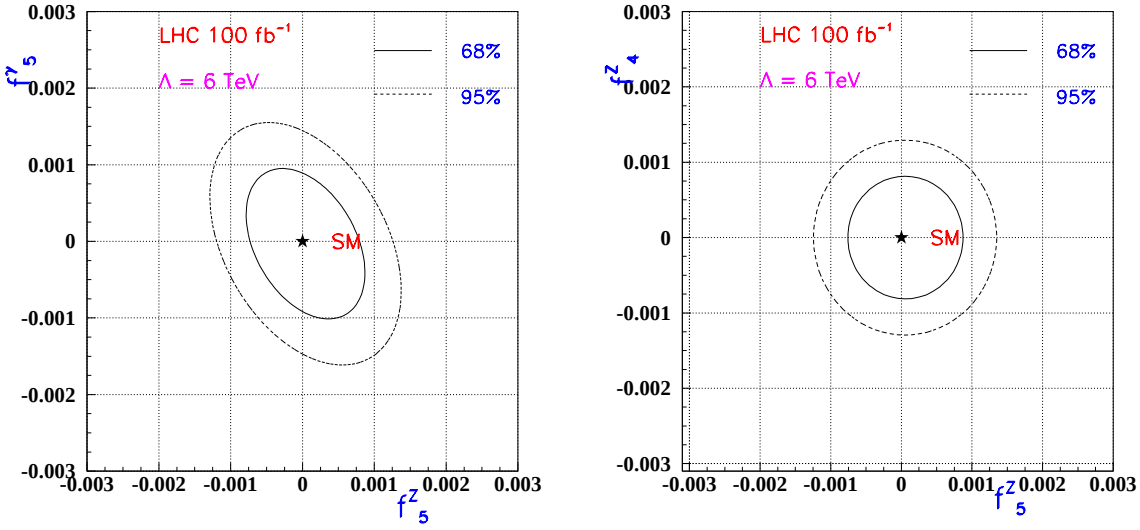

Figure 19: *Two-dimensional sensitivity limits for pairs of NTGCs in* $ZZ \to \ell^+\ell^-\ell^+\ell^-(l = e, \mu)$ *for an integrated luminosity of* $100\, fb^{-1}$. *The 68% and 95% confidence level contours are shown for all combinations of couplings. A form factor scale of* $\Lambda_{FF} = 6\, TeV$ *has been assumed. In each graph, only those couplings which are plotted against each other are assumed to be different from their zero SM values.*

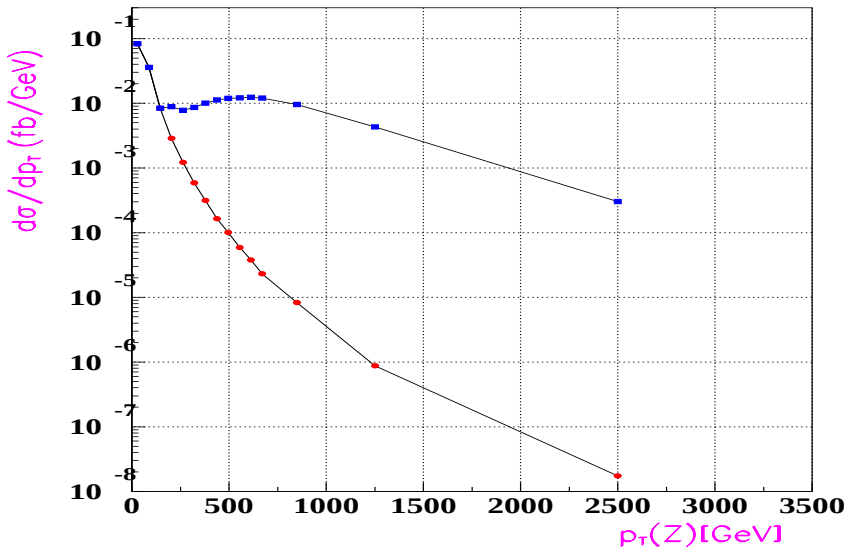

Figure 20: *Distribution of the differential cross section of the* $ZZ \to \ell^+\ell^-\ell^+\ell^-(l = e, \mu)$ *as a function of* $p_T(Z)$ *in the case of the SM (lower line) and for* $f_4^{\gamma} = 0.02$. $\Lambda_{FF} = 6\, TeV$

(The LEP2 limits do not contain any form factor effect). In Run II at the TeVatron, CDF and DØ will improve these bounds by at least a factor 4 [23].
The LHC will be able to improve these bounds by a factor 1000 approximately and become almost sensitive to radiative corrections in the SM and to contributions from

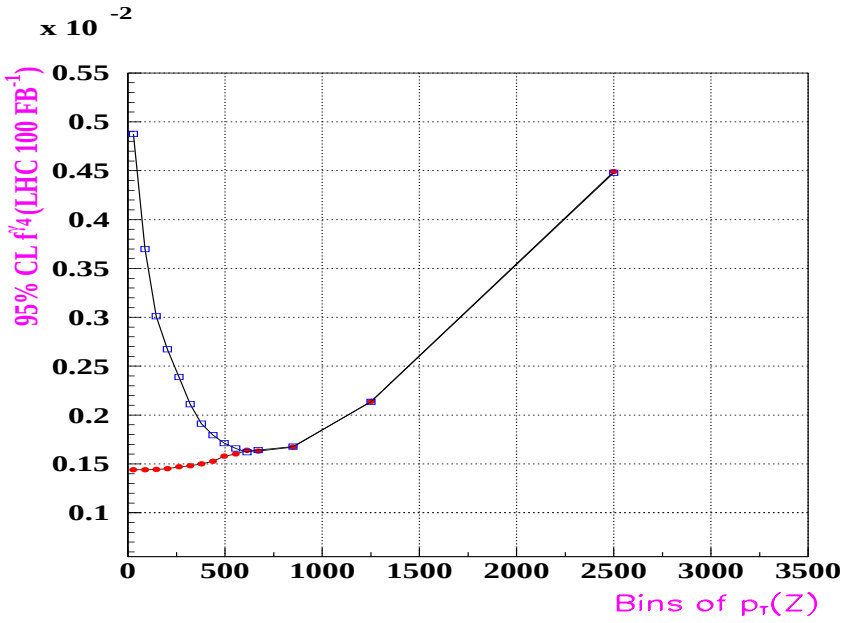

Figure 21: *Limits on f_4^γ versus $p_T(Z)$ threshold using the counting method (squares) and a binned fit to $p_T(Z)$ (circles) in $ZZ \to \ell^+\ell^-\ell^+\ell^-(l = e, \mu)$ channel. The lines are drawn to guide the eye.*

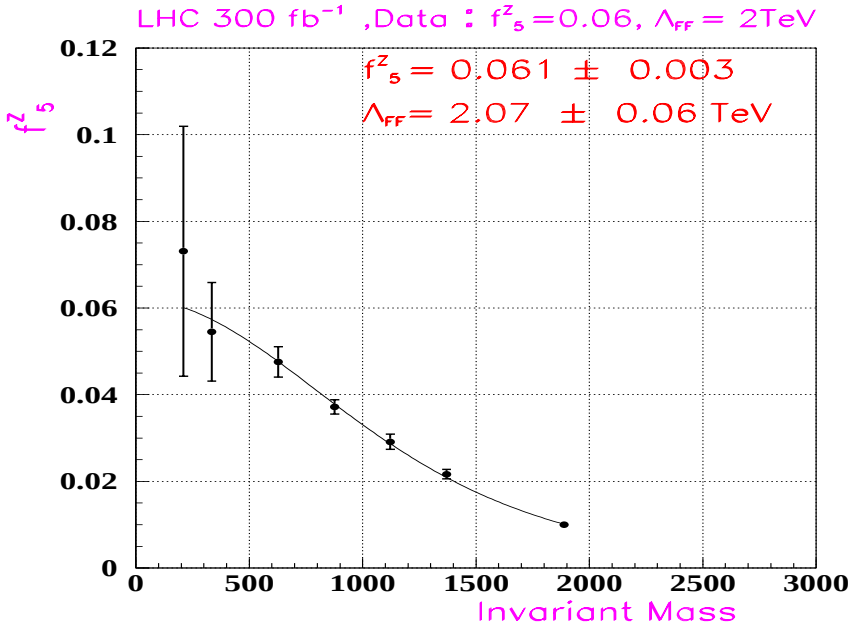

Figure 22: *The f_5^Z form factor is extracted in restricted invariant mass domains for 300 fb^{-1} of LHC data, assuming nature provides an anomalous $f_{50}^Z = 0.06$ described by $n = 3$ dipole form factor with $\Lambda_{FF} = 2TeV$. A fit to a $n = 3$ dipole form factor is performed to reconstruct the bare coupling and form factor scale.*

supersymetric models.
One may also note that at the LC [5], the 68% confidence level limits for f_4^γ, f_4^Z, f_5^γ, f_5^Z

are about 2×10^{-3}, 4×10^{-4}, 3×10^{-3}, 7×10^{-4}, respectively similar or worse than the LHC sensitivity limits.

The study presented in this note was done in leading order, since a jet veto removes NLO effects. The limits obtained for all four of the NTGCs are similar, because all four operators have the same dimensionality, unlike the WV case. Although the LHC luminosity will allow binning in several dimensions, the use of multi-dimensional log-likelihood determination does not significantly improve the results obtained using a one-dimensional $p_T(Z)$ distribution.

Acknowledgments

I would like to thank L. Fayard for many stimulating and helpful discussions. I thank J.B. Hansen for a very careful and detailed reading of this note and for his very valuable comments. I also thank F. Gianotti for fruitful discussions and useful comments as well as G. Azuelos and M. Dobbs for reading this note and making valuable suggestions.

References

[1] K. Hagiwara, R.D. Peccei, D. Zeppenfeld and K.Hikasa, Nucl.Phys.B282 (1987)253.
K. J. F. Gaemers and G.J. Gounaris, Z.Phys.C1 (1979) 259.

[2] For a review of charged boson TGC at LEP see
S.Jezequel LAPP-EXP-2000-10, talk given at ICHEP2000, 27 July -2 August 2000, Osaka, Japan.
For a review of neutral boson TGC see C. Matteuzzi, talk given at ICHEP2000, 27 July -2 August 2000, Osaka, Japan.
A. Oh, talk given at EPS 2001, July 12-18, 2001 Budapest, Hungary.

[3] D. Benjamin, for the CDF Collaboration, Fermilab-conf-95/241-E
B. Abbott et al (D0 Collaboration), Phys.Rev.D60 (1999)072002;Phys.Rev.D57 (1998)3817.
A. Abachi et al (D0 Collaboration), Phys.Rev.D56 (1997) 6742.

[4] G.J. Gounaris, J. Layssac and F.M. Renard, Phys.Rev.D61 (2000) 073013; Phys.Rev.D62 (2000) 073013.

[5] D. Chang, W-Y Keung and P. B. Pal, Phys.Rev.D51 (1995)1326.

[6] ATLAS Collaboration, Detector and Physics Performance, Technical Design Report, Section 16. 2, CERN/LHCC/99-15 (1999).
Proceeding of the Workshop on Standard Model Physics (and more) at the LHC, G. Altarelli and M. L Mangano (eds) CERN 2000-004 p169.
D. Fouchez, Atlas Internal note PHYS-NO-060 (Jan 1995).

M. Dobbs and J.B. Hansen, Transparencies shown at the ATLAS Plenary Physics meeting of 10-02-2000.

[7] T.G. Rizzo, Phys.Rev.D32 (1985)43.

[8] U. Baur and D. Zeppenfeld, Phys Lett B201 (1988)383.

[9] U. Baur and D. Rainwater, Phys.Rev.D62 (2000)113011

[10] B. Mele, P. Nason and G. Ridolfi, Nucl.Phys.B357 (1991)409.
J. Ohnemus and J.F. Owens, Phys.Rev.D43 (1991)3626.
J. Ohnemus, Phys.Rev.D50 (1994)1931;hep-ph/9503389.
S. Frixione, P. Nason and G. Ridolfi, Nucl.Phys.B383 (1992)3.

[11] R.W. Brown, D. Sahdev and K.O. Mikaelian, Phys.Rev.D20 (1979)1164.
K.O. Mikaelian M.A. Samuel and D. Sahdev, Phys.Rev.Lett 43 (1979)746
U. Baur, T. Han and J. Ohnemus, Phys.Rev.Lett 72 (1994)3941.

[12] U. Baur, T. Han and J. Ohnemus, Phys.Rev.D51 (1995)3381.

[13] L. Dixon, Z. Kunszt and A. Signer, Phys.Rev.D60 (1999)114037.

[14] U. Baur, private communication. See however: EWN Glover and JJ van der Bij Phys Lett B219 (1989)488 where this contribution was found $\sim 40\%$.

[15] T. Sjostrand, 'Pythia 5. 7 and Jetset 7. 4: Physics and manual' LU-TP-95-20 (1995).

[16] E. Richter-Was, D. Froidevaux and L. Poggioli, 'ATLFAST 2. 0 a fast

[17] Kersevan, B P ; Richter-Was, E. The gg, qqbar - Z/gamma*(- l l) b bbar process: matrix element implementation to PYTHIA6.1 ATL-PHYS-2001-021

[18] Package for the single top quark production at hadron colliders, provided by the "Top Working Group".

[19] D. Costanzo private communication.
V. Cavasini, D. Costanzo, I. Vivarelli, ATL-COM-PHYS-2002-004.

[20] ATLAS Collaboration, Detector and Physics Performance, Technical Design Report, Section 9. 2. 2 p291, CERN/LHCC/99-14 (1999).

[21] ATLAS Collaboration, Detector and Physics Performance, Technical Design Report, Section 13 p433, CERN/LHCC/99-14 (1999).

[22] Talk given by Jorgen Beck Hansen at LC Workshop, Obernai October 16-19 1999.

[23] QCD and Weak Boson Physics in Run II , U. Baur, R.K. Ellis and D.Zeppenfeld (eds) Fermilab-Pub-00/297, hep-ph/0005226.